Atmos. Chem. Phys., 26, 11785–11802, 2026
https://doi.org/10.5194/acp-26-11785-2026

Atmospheric Chemistry and Physics
Open Access
EGU

Measurement Report: Quantitative analysis of aerosol acidity and its driving factors in Guanzhong area, Northwest China

Qian Wang[1,2], Xiao Guo[1], Minxia Shen[1], Yali Liu[3], Yifan Zhang[3], Lu Li[1], Weining Qi[1,2], Yue Cao[3], Shicong Li[1], Zhuoer Dong[1,2], Wenting Dai[1,4], and Jianjun Li[1,4]

[1]State Key Laboratory of Loess Science, Institute of Earth Environment, Chinese Academy of Sciences, Xi'an, China
[2]University of Chinese Academy of Sciences, Beijing, China
[3]Xi'an Institute for Innovative Earth Environment Research, Xi'an, China
[4]National Field Observation and Research Station (Shaanxi) for Ecological and Environment Changes and Integrated Management in the Guanzhong Plain Region, Xi'an, China

Correspondence: Jianjun Li (lijj@ieecas.cn)

Received: 2 February 2026 – Discussion started: 16 February 2026
Revised: 30 May 2026 – Accepted: 3 August 2026 – Published: 20 August 2026

Abstract. Aerosol acidity significantly affects atmospheric chemistry and human health, yet its driving factors remain controversial. This study systematically examined a year-long characteristics of water-soluble inorganic ions in $PM_{2.5}$ in the semi-arid Guanzhong Plain, Northwest China, and quantitatively analyzed its acidity and driving factors. The annual mean pH of $PM_{2.5}$ was 3.8 ± 1.0 (winter > spring > summer > autumn). As pollution increased, aerosol pH shifted from the acidic range (2–5) on clean days to a near-neutral range (3–6) on polluted days. Sensitivity tests and driver analysis revealed that atmospheric temperature (22.3 %–33.8 %), NH_x (gas NH_3+NH_4^+, 11.4 %–44.9 %), and SO_4^{2-} (8.5 %–10.8 %) were common key factors influencing pH across all seasons, with the percentages representing the quantitative contribution of each factor to the overall pH variation. Among these, temperature played a dominant role in seasonal variations, while NH_x was the primary contributor during autumn and winter. Notably, Ca^{2+} emerged as a unique driver specific to spring, the relative standard deviation (RSD) was 8.8 %, indicating a substantial impact of Ca^{2+} variability on spring aerosol pH. Relative humidity (RH) exhibited a distinctive non-linear regulatory effect, i.e., aerosol pH initially decreases and subsequently increases with rising RH (inflection point occurred at 60 %–85 %). This phenomenon is primarily attributed to an abrupt change in liquid water content triggered by the deliquescence of hygroscopic components. Our results enhance the understanding of the contributions of various factors to aerosol pH.

1 Introduction

Atmospheric aerosols play a vital role in the Earth's atmospheric system, significantly impacting regional and global air quality, climate change, and human health (Liu et al., 2025b; Zhang et al., 2017). Among these properties, aerosol acidity, typically characterized by pH, is one of the most critical parameters. Research indicates that acidity can directly or indirectly regulate the gas-particle partitioning of semi-volatile species and the rates of chemical reactions (Guo et al., 2016; Paglione et al., 2021). It drives pH-dependent aqueous-phase reactions and impacts other processes related to particle formation and growth. Additionally, acidity can enhance the formation of secondary organic aerosol (SOA) and influence its transformation pathways through acid-catalyzed reactions (Rengarajan et al., 2011; Shi et al., 2019). Moreover, aerosol pH affects the dissolution of trace metals and the concentration of their toxic forms, with stronger acidity promoting metal dissolution via acid dissociation (Ding et al., 2019; Shi et al., 2011). High aerosol

acidity levels not only increase the risks of respiratory illnesses and specific cancers but also drive atmospheric processes that lead to complex air pollution, dry and wet deposition of pollutants, and ultimate impacts on human health and the climate system (Mao et al., 2009; Pye et al., 2020). Therefore, the exploration of particle pH is crucial for enhancing air quality management strategies and policy development, which is highly important for alleviating the health and environmental consequences of air pollution. The direct measurement of atmospheric aerosol acidity presents challenges (Xu et al., 2025), primarily due to the difficulties in quantifying the aqueous-phase concentrations of semi-volatile compounds and H^+ in ambient particulate matter. Thus, thermodynamic models, such as E-AIM (Clegg et al., 1998) and ISORROPIA (Nenes et al., 1998), were frequently used as a proxy method for assessing aerosol acidity in recent decades.

Aerosol acidity displays notable spatiotemporal variability, playing a crucial role in atmospheric environmental research. Globally, aerosols in Europe and North America generally exhibit higher acidity levels compared to those in China, with pH values 1–2 units lower (Zhang et al., 2021a). In North America, coastal cities in Canada frequently exhibit greater aerosol acidity than inland regions, primarily due to elevated humidity that enhances the aqueous-phase oxidation of SO_2 (Brook et al., 1997). In China, aerosol acidity typically rises from north to south. Specifically, during winter in the heavily polluted North China Plain, pH values typically range from 4.1 to 4.9 (Ding et al., 2019; Liu et al., 2017; Shi et al., 2019; Tan et al., 2018). In the Guanzhong region, aerosol pH can reach as high as 5 (Wang et al., 2016). Conversely, coastal cities in southeastern China, such as Guangzhou and Xiamen, display significantly lower mean pH values of 2.5 and 3.5, respectively (Jia et al., 2020; Xu et al., 2025). Furthermore, vertical differences in aerosol acidity are also noteworthy. As altitude increases, aerosol acidity generally intensifies, with higher acidity observed at mountain summits compared to surface levels (Feng et al., 2023; Guo et al., 2016). Temporally, aerosol acidity is typically higher in summer than in winter, while patterns in spring and autumn fluctuate based on regional climatic and emission characteristics (Tan et al., 2018; Xu et al., 2025). In recent years, aerosol acidity has gained prominence in academic research and discussion due to its critical role in influencing aerosol physicochemical properties (Cui et al., 2025; Liu et al., 2021; Paglione et al., 2021; Tao et al., 2025). However, its levels are governed by numerous, complex, and region-dependent factors, leading to significant spatial heterogeneity. Therefore, investigating the dynamic changes in aerosol acidity throughout different seasons and understanding the underlying mechanisms are crucial for enhancing our comprehension of haze formation and developing precise air pollution control strategies.

Through quantitative analysis of aerosol pH driving factors and elucidation of $PM_{2.5}$ chemical composition and meteorological impacts across seasons, we can better understand spatiotemporal variation pattern (Jia et al., 2020; Xu et al., 2025). Previous studies showed that in Beijing, SO_4^{2-}, NH_x, and T significantly affect $PM_{2.5}$ pH, while Ca^{2+} and RH serve as dominant factors in spring and summer, respectively (Ding et al., 2019). In contrast, in southeastern Chinese cities such as Guangzhou and Xiamen, meteorological parameters like T and RH exert an even greater influence on pH variation than chemical components (Jia et al., 2020; Xu et al., 2025). These findings underscore the complexity of the factors influencing aerosol acidity. However, existing studies have largely focused on compositional analyses in specific cities, resulting in both a lack of year-round quantitative attribution of pH drivers in semi-arid regions, insufficient comparison of chemical versus meteorological contributions, and neglect of alkaline dust, as well as an overall insufficient understanding of the trends in aerosol pH values and their primary driving factors and relative contributions.

Guanzhong Plain is a vital economic and agricultural center in northwestern China, where rapid industrial and urban development has resulted in severe air pollution complexities. The mechanisms of air pollution formation and its driving factors in the region are significantly shaped by its inland geographical characteristics and socio-economic conditions. The unique semi-enclosed topography, with the Loess Plateau to the north and the Qinling Mountains to the south, restricts pollutant dispersion, leading to the accumulation of various pollutants and enabling complex chemical reactions (Huang et al., 2014; Liu et al., 2025b; Shen et al., 2024). This confinement likely amplifies the influence of local emissions on aerosol pH due to the accumulation of both acidic and alkaline species. The area is known for its intensive agricultural practices, contributing to high levels of ammonia emissions that influence aerosol acid-base equilibrium. The ammonia-rich condition likely neutralizes acidic components, thereby shifting aerosol pH toward a weaker acidic range (Liu et al., 2019). Additionally, long-distance transportation from the nearby Loess Plateau introduces alkaline mineral dust and crustal cations (e.g., Ca^{2+}, Mg^{2+}) that can neutralize acidic components effectively. Furthermore, seasonal variation of meteorological conditions also influences the transformation and removal processes of pollutants. The combination of these factors makes the Guanzhong Plain a unique location for a comprehensive study on aerosol pH trends and key influencing factors, which would differ from those in southeastern coastal cities of China, where marine air masses and hot, humid meteorological conditions predominantly influence air quality.

In this study, we conducted a year-long observation of water-soluble inorganic compositions of $PM_{2.5}$ in the Guanzhong region, and utilized an ISORROPIA-II model to access aerosol pH and liquid water content. The primary objectives of this study are: (1) to characterize the seasonal variation of aerosol acidity in the Guanzhong Plain and to examine its evolution under varying pollution levels; and (2) to identify the key driving factors influencing aerosol pH in

each season and to quantify their relative contributions across different seasons.

2 Materials and Methods

2.1 Sample collection

$PM_{2.5}$ samples were collected at the National Field Observation and Research Station (Shaanxi) for Ecological and Environment Changes and Integrated Management in the Guanzhong Plain Region, Xi'an, China (34°3′39″ N, 108°20′37″ E; 503 m a.s.l.). This station is positioned at the northern foothills of the Qinling Mountains (Fig. 1) and functions as a regional background site. It is located approximately 60 km southwest of Xi'an city, with no significant industrial, traffic, or other substantial anthropogenic pollution sources. The sampling campaign spanned from 1 January to 21 December 2022, and a total of 295 valid samples were obtained during the study. Daily sampling was conducted from 10:00 to 09:00 the next day, lasting for 23 h. Samples were collected using a medium-flow sampler (HC-1010, China Qingdao Company, China) equipped with quartz fiber filters (Whatman QMA, USA) with pre-baked (450 °C, 5 h) quartz fiber filters (Whatman, QMA, USA) at an airflow rate of 100 L min^{-1}. After sampling, each filter sample was promptly enveloped in aluminum foil, sealed, and frozen at −20 °C for subsequent laboratory analysis. To ensure quality control, field blank samples were collected both before and after sampling. This involved placing pretreated blank filters into the sampler, allowing them to stand for 10 min without activating the pump, and then sealing and storing them using the same procedure as the actual samples. The chemical analysis data for all samples were adjusted by deducting the average concentration measured from the two blank samples to eliminate potential systematic errors.

Daily average concentrations of PM_{10}, SO_2, NO_2, CO, and O_3-8 h (defined as the maximum 8 h average O_3 concentration) were obtained from the local government. Meteorological parameters, including ambient temperature (T), relative humidity (RH), wind speed (WS), and atmospheric pressure (AP), were acquired from the National Observation and Research Station for Regional Ecological Environment Change and Comprehensive Management in the Guanzhong Plain, Shaanxi Province, China.

2.2 Analysis of water-soluble inorganic ions and ammonium partitioning ratio

Water-soluble inorganic ions (WSIIs), including SO_4^{2-}, NO_3^-, NH_4^+, Cl^-, Ca^{2+}, K^+, Mg^{2+}, and Na^+, were analyzed using ion chromatography (Metrohm-940, Switzerland). To enhance measurement accuracy, a fixed amount of lithium bromide was added to the eluent. For quality assurance, one sample out of every ten was randomly selected for re-analysis. All WSII concentrations were corrected using field blanks, which exhibited concentrations less than 10 % of those in ambient samples. The limits of detection (LODs) for SO_4^{2-}, NO_3^-, NH_4^+, Cl^-, Ca^{2+}, K^+, Mg^{2+}, and Na^+ were 0.027, 0.026, 0.0010, 0.0087, 0.0012, 0.0011, 0.0008, and 0.0005 μg m^{-3}, respectively (Liu et al., 2025b). The mass concentrations of all detected WSIIs were significantly higher than their corresponding LODs.

As detailed in the preceding section, this study employed ammonium partitioning ratio (NHR) to quantify the transformation of gaseous ammonia into particulate ammonium (Xie et al., 2020; Zhang et al., 2021b). This ratio is defined as the molar concentration of particulate ammonium ($n(NH_4^+)$, μmol m^{-3}) relative to the total molar concentration of inorganic ammonium ($n(NH_3) + n(NH_4^+)$, μmol m^{-3}), calculated using the following equation:

$$\mathrm{NHR} = \frac{n(\mathrm{NH_4^+})}{n\left(\mathrm{NH_4^+}\right) + n(\mathrm{NH_3})} \quad (1)$$

2.3 Calculation of aerosol pH

In this study, the ISORROPIA-II model was utilized to estimate aerosol thermodynamic parameters. The model was operated in "forward" mode, based on the assumption that aerosols were in a "metastable" state (Fountoukis and Nenes, 2007; Nenes et al., 1998), with inputs including concentrations of SO_4^{2-}, NH_x, NO_3^-, Cl^-, Na^+, Ca^{2+}, K^+, Mg^{2+}, RH and T. Aerosol pH was calculated using the following equation:

$$\mathrm{pH} = -lg\frac{1000\gamma_{\mathrm{H^+}}\mathrm{H_{air}^+}}{\mathrm{ALWC}} \quad (2)$$

where γ_{H^+} is the hydronium ion activity coefficient (assumed = 1), H_{air}^+ (μg m^{-3}) indicates the concentration of hydronium ions per unit volume of air, and ALWC (μg m^{-3}) signifies the aerosol liquid water content. It should be noted that the model-calculated pH values are more reliable when the RH falls within the range of 30 % to 95 % (Guo et al., 2016).

Neglecting the influence of gaseous species, such as NH_3, HNO_3, and HCl, on aerosol acidity often results in an underestimation of acidity. The effect of these gases on aerosol pH can only be dismissed when their atmospheric concentrations are exceedingly low (Guo et al., 2015; Hennigan et al., 2015). In China, atmospheric ammonia concentrations are relatively high, and the study region is characterized by elevated ammonia levels; thus, NH_3 cannot be overlooked. In this study, We modified the method of Wei et al. (2023) by shifting the prediction target from NH_3 to NHR. Based on our earlier datasets (Wu et al., 2020), we performed multiple linear regression to estimate NHR, which was subsequently used to retrieve NH_3 levels. However, previous research has shown that the concentrations of gaseous HNO_3 and HCl in urban Xi'an remained below 1 μg m^{-3} throughout all seasons. Since the Qinling site serves as a background location, concentrations there are anticipated to be even lower. Given

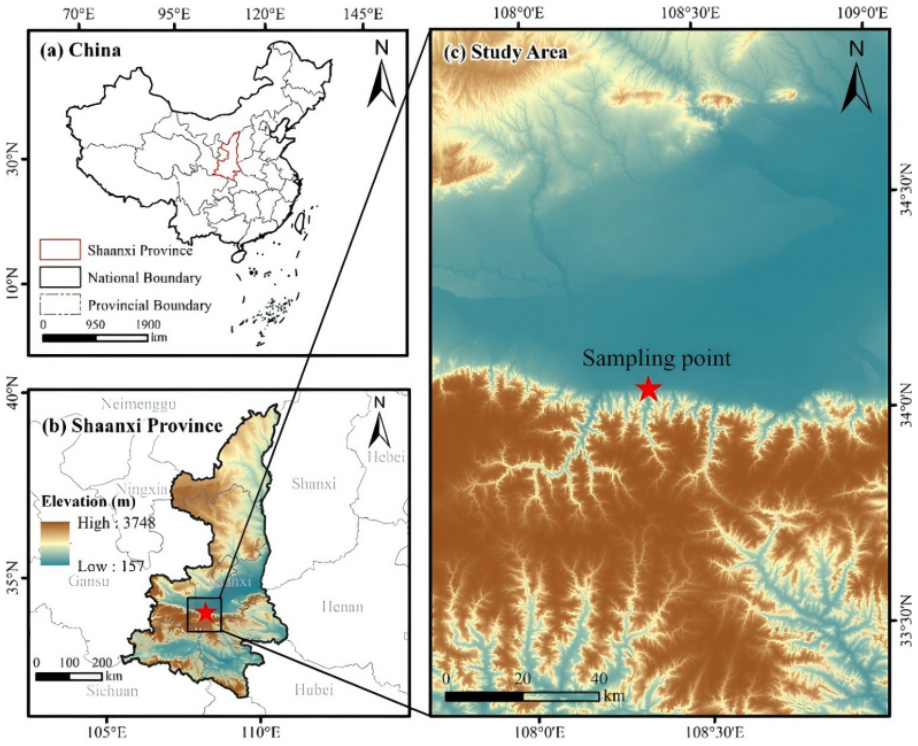

Figure 1. Locations of monitoring stations in Qinling.

these negligibly low levels, we utilized the measured concentrations of particulate NO_3^- and Cl^- as inputs for TNO_3 and TCl, respectively (Nah et al., 2023).

2.4 Multiple linear regression model

In ammonia-rich regions, aerosol pH, particularly during winter, is primarily influenced by NH_3 levels (Tao and Murphy, 2019). However, the frequent absence of long-term and continuous NH_3 observational data impedes the analysis of long-term trends in $PM_{2.5}$ chemical properties. To fill this data gap and explore variations in aerosol pH in the research area, this study aimed to create a model for estimating the NHR based on easily accessible routine monitoring data to estimate NH_3 concentrations. Given the well-established thermodynamic and chemical relationships between NHR and factors such as NO_3^-, SO_4^{2-}, and T (Fountoukis and Nenes, 2007), all parameters that serve as inputs to the thermodynamic model ISORROPIA-II, were included as candidate independent variables. Multiple linear regression (MLR) was performed using SPSS software with NHR as the dependent variable, and the model parameters were estimated using ordinary least squares.

The model was trained using a previous high-resolution (1 h) online $PM_{2.5}$ dataset from an urban site in Xi'an during 2016–2017 (Wu et al., 2020), which included major WSIIs concentrations in $PM_{2.5}$, NH_3 concentrations, and meteorological data (T and RH) from the same observation site. The data covered all four seasons: winter ($n = 605$, from 21 December 2016 to 23 January 2017), spring ($n = 704$, from 31 March to 30 April 2016), summer ($n = 591$, from 8 July to 6 August 2017), and autumn ($n = 1032$, from 1 October to 15 November 2017). Following model construction, its validity and accuracy were systematically assessed using the correlation coefficient, the F-test, and the T-test (Wei et al., 2023). For variables with $p > 0.05$, they were retained to preserve model integrity, as they may indirectly influence NHR and were shown to have a negligible effect on pH verified by comparison (Table S1 in the Supplement). Despite the variations in ion concentrations between the training data and our study site, the thermodynamic mechanism that governs NHR remains consistent across different concentration levels. Furthermore, the ranges of the key input variables encompass the observed values at our site. Consequently, the model trained on urban data can be effectively utilized to predict NHR at the background site.

2.5 Sensitivity tests and quantitative analysis

This study assessed the impact of various factors on aerosol pH through sensitivity tests. The variables analyzed included meteorological parameters (T, RH) and chemical components (SO_4^{2-}, NH_x, NO_3^-, Cl^-, Na^+, Ca^{2+}, K^+, Mg^{2+}) (Tao and Murphy, 2019). The specific sensitivity analysis adhered to the methodology outlined by Ding et al. (2019): Within the ISORROPIA-II model, the measured value of a target

variable i was used sequentially as input alongside the average values of all other parameters. By observing the resulting trend in the output pH, the individual effect of variable i on aerosol pH could be assessed.

To quantitatively evaluate the influence of each factor on aerosol pH, two complementary approaches were utilized: the relative standard deviation (RSD) method and the ΔpH contribution decomposition method. The RSD, which is derived from the coefficient of variation of pH responses in sensitivity analysis (the ratio of standard deviation to mean), indicates the relative sensitivity of aerosol pH to typical fluctuations of a given factor; a higher RSD signifies a greater potential impact. However, the RSD method provides only a relative ranking and does not directly determine the absolute contribution of each factor to the observed pH. Consequently, this study emphasizes the quantitative analysis of ΔpH contributions quantitative analysis.

Assuming the aerosol pH estimated under scenario 1 (pH_1) differed from that under scenario 2 (pH_2), the pH difference ($\Delta pH = pH_2 - pH_1$) was thus caused by the variations in the factors listed above. The quantitative analysis method adhered to the approach outlined by Zhou et al. (2022). To quantify the contribution of a single variable j within the ISORROPIA-II model, the value of factor j was altered from its Scenario 1 value to its Scenario 2 value, while all other parameters remained constant. The resulting change in pH was recorded as ΔpH_j, which represents the independent contribution of that specific factor to the total ΔpH. In this study, the aforementioned method was applied to consecutive seasonal pairs in the following order: spring values were substituted into the winter scenario, summer values into spring, autumn values into summer, and winter values into autumn (Table S2). For each pairwise substitution, Scenario 2 denotes the season being introduced, while Scenario 1 refers to the base season. Consequently, the calculated ΔpH quantifies the impact of each factor's seasonal shift on aerosol pH. The remaining change in pH, not accounted for by this procedure, is attributed to ΔpH_{others}, reflecting the combined effects of synergistic variations among the factors.

3 Results and discussion

3.1 Seasonal variations in $PM_{2.5}$ and its chemical composition

3.1.1 Seasonal variations in $PM_{2.5}$ and air pollutants

The annual variation for $PM_{2.5}$ mass concentrations, gaseous pollutants (SO_2, CO, NO_2, and O_3-8 h), and meteorological parameters (T, RH, WS, and AP) are shown in Fig. 2, with seasonal statistics summarized in Table 1. The sampling period in 2022 was categorized into four seasons based on local heating patterns and human activity trends: winter (1 January to 12 March, and 15 November to 21 December), spring (16 March to 31 May), summer (1 June to 30 August), and autumn (1 September to 14 November). During the observation period, the $PM_{2.5}$ mass concentration varied from 9.8 to 221.7 $\mu g\,m^{-3}$, with an annual mean of $65.3 \pm 61.8\,\mu g\,m^{-3}$. This concentration is lower than those reported for other typical areas in the Guanzhong Plain (Liu et al., 2025b; Zhang et al., 2019), aligning with expectations of minimal local emission influence at this site. In comparison to the annual mean of 105.6 $\mu g\,m^{-3}$ recorded at a Qinling background station in 2012 (Niu et al., 2016), the concentration observed in this study is approximately 36 % lower, suggesting a significant reduction in air pollution in recent years due to effective air quality control measures. $PM_{2.5}$ concentrations exhibited marked seasonal variations, showing the seasonal order of winter ($93.5 \pm 41.7\,\mu g\,m^{-3}$) > spring ($61.4 \pm 40.8\,\mu g\,m^{-3}$) > autumn ($43.1 \pm 25.1\,\mu g\,m^{-3}$) > summer ($33.2 \pm 13.7\,\mu g\,m^{-3}$). The majority of days exceeding the daily $PM_{2.5}$ limitation (Grade II, 75 $\mu g\,m^{-3}$) from the ambient air quality standards of China occurred in winter, with about 68 % of daily average concentrations surpassing the limitation (Table S3). This trend underscores the significant influence of heating activities and adverse meteorological conditions on air quality.

The concentrations of gaseous pollutants also demonstrated significant seasonal variations. CO and NO_2, primary pollutants mainly from fossil fuel combustion, had higher levels in autumn and winter and lower levels in spring and summer, particularly elevated during the heating period compared to the non-heating period. This pattern is linked to increased emissions during heating demands in autumn and winter, along with unfavorable meteorological conditions hindering pollutant dispersion (Liu et al., 2025b). Due to its strong dependence on solar radiation intensity and temperature, O_3-8 h value peaked in July during summer (156.8 $\mu g\,m^{-3}$) and subsequently decreased as sunlight weakened with varying intensity. This anti-phase variation underscores the seasonal differences in the dominant formation mechanisms for different pollutants.

3.1.2 Water-soluble inorganic ions in $PM_{2.5}$

The concentrations of WSIIs (SO_4^{2-}, NO_3^-, NH_4^+, Cl^-, Ca^{2+}, K^+, Mg^{2+}, Na^+) in $PM_{2.5}$ are shown in Fig. 2 and Table 1. The annual average concentration of total measured WSIIs was $24.5 \pm 20.5\,\mu g\,m^{-3}$, representing approximately 38 % of the $PM_{2.5}$ mass. Significant seasonal variations were noted, with concentrations following the order: winter ($39.5 \pm 22.0\,\mu g\,m^{-3}$) > autumn ($19.8 \pm 15.9\,\mu g\,m^{-3}$) > spring ($18.6 \pm 12.9\,\mu g\,m^{-3}$) > summer ($8.5 \pm 4.2\,\mu g\,m^{-3}$). Among the WSIIs, secondary inorganic aerosols (i.e., SO_4^{2-}, NO_3^-, and NH_4^+ (SNA)) were the predominant constituents, collectively contributing 89.0 % to the total WSIIs. This SNA-dominated composition suggests that aerosol pH is regulated by the neutralization balance between NH_4^+ and the acidic anions SO_4^{2-} and NO_3^-, thereby laying a chemical foundation for the analysis of seasonal driving factors. No-

Table 1. Concentrations of air pollutants, meteorological parameters, chemical components and ammonia-related species (NHR from multiple linear regression and NH_3 from back-calculates of NHR, NH_x = gas NH_3+NH_4^+) in different seasons.

	Annual	Winter	Spring	Summer	Autumn
$PM_{2.5}$ ($\mu g\,m^{-3}$)	65.3 ± 61.8	93.5 ± 41.7	61.4 ± 40.8	33.3 ± 13.7	43.1 ± 25.1
PM_{10} ($\mu g\,m^{-3}$)	97.5 ± 66.3	146.0 ± 61.1	87.7 ± 66.6	39.3 ± 14.3	94.2 ± 49.1
T (K)	289.3 ± 10.1	278.2 ± 4.2	291.1 ± 5.3	302.0 ± 4.0	290.3 ± 5.1
RH (%)	66.5 ± 20.2	65.5 ± 20.9	62.2 ± 19.8	61.2 ± 19.1	80.0 ± 14.8
WS ($m\,s^{-1}$)	0.7 ± 0.3	0.7 ± 0.2	0.8 ± 0.3	0.9 ± 0.3	0.6 ± 0.2
SO_2 ($\mu g\,m^{-3}$)	8.9 ± 4.6	10.0 ± 4.5	4.9 ± 2.0	8.6 ± 3.4	11.9 ± 5.0
CO ($mg\,m^{-3}$)	0.7 ± 0.4	1.1 ± 0.5	0.5 ± 0.1	0.4 ± 0.1	0.6 ± 0.2
NO_2 ($\mu g\,m^{-3}$)	25.9 ± 15.1	37.4 ± 13.2	25.0 ± 8.4	9.8 ± 4.5	26.4 ± 14.4
O_3 ($\mu g\,m^{-3}$)	99.6 ± 50.1	67.8 ± 33.2	109.5 ± 40.2	150.2 ± 43.2	83.4 ± 39.7
WSIIs ($\mu g\,m^{-3}$)	24.5 ± 20.5	39.5 ± 22.0	18.6 ± 12.9	8.5 ± 4.2	19.8 ± 15.9
SNA ($\mu g\,m^{-3}$)	21.8 ± 19.4	35.5 ± 21.1	16.1 ± 12.3	7.0 ± 3.7	18.1 ± 15.5
SO_4^{2-} ($\mu g\,m^{-3}$)	5.1 ± 3.7	7.3 ± 4.7	4.1 ± 1.7	3.4 ± 2.1	4.4 ± 3.1
NO_3^- ($\mu g\,m^{-3}$)	8.8 ± 10.8	16.3 ± 11.9	6.1 ± 7.0	1.0 ± 1.2	8.7 ± 10.8
NH_4^+ ($\mu g\,m^{-3}$)	4.0 ± 4.7	7.3 ± 5.7	2.4 ± 2.6	1.1 ± 0.8	3.8 ± 4.1
Cl^- ($\mu g\,m^{-3}$)	0.5 ± 0.7	1.1 ± 0.8	0.3 ± 0.2	0.1 ± 0.1	0.3 ± 0.3
Ca^{2+} ($\mu g\,m^{-3}$)	1.4 ± 1.6	1.8 ± 1.8	1.9 ± 1.6	0.8 ± 0.6	0.6 ± 0.3
K^+ ($\mu g\,m^{-3}$)	0.3 ± 0.4	0.6 ± 0.4	0.2 ± 0.1	0.1 ± 0.1	0.2 ± 0.2
Mg^{2+} ($\mu g\,m^{-3}$)	0.1 ± 0.1	0.2 ± 0.1	0.2 ± 0.1	0.1 ± 0.1	0.1 ± 0.1
Na^+ ($\mu g\,m^{-3}$)	0.7 ± 0.4	0.9 ± 0.5	0.7 ± 0.2	0.6 ± 0.2	0.6 ± 0.1
NH_3 ($\mu g\,m^{-3}$)	12.8 ± 10.3	22.6 ± 10.0	5.9 ± 4.3	12.1 ± 5.5	4.5 ± 3.9
NH_x ($\mu g\,m^{-3}$)	16.7 ± 14.1	29.7 ± 15.1	8.3 ± 6.8	13.2 ± 6.3	8.4 ± 7.9
NHR	0.2 ± 0.1	0.2 ± 0.1	0.2 ± 0.1	0.1 ± 0.1	0.4 ± 0.1

tably, NO_3^- exhibited the highest concentration ($8.8\,\mu g\,m^{-3}$, 35.9 %), followed by SO_4^{2-} ($5.1\,\mu g\,m^{-3}$, 20.7 %) and NH_4^+ ($4.0\,\mu g\,m^{-3}$, 16.3 %), indicating nitrate as the most abundant ionic species. This might be driven by enhanced atmospheric oxidation and rising ammonia emissions via pathways like OH radical and N_2O_5 reactions. Nitrate dominance, as opposed to sulfate-dominated conditions, indicates a stronger reliance of aerosol acid-base balance on the partitioning of semi-volatile NH_4NO_3. This partitioning process is highly sensitive to ambient temperature, relative humidity, and ammonia concentration, which may result in greater dynamic variations in aerosol pH (Song et al., 2019; Guo et al., 2016).

The ternary plot in Fig. S1 in the Supplement illustrates the molar concentration ratios of SO_4^{2-}, NO_3^-, and NH_4^+ across seasons. The proportion of NO_3^- within SNA was markedly greater in winter compared to summer, while the situation was reversed for SO_4^{2-}. These seasonal fluctuations primarily stem from the thermal instability and volatility of NH_4NO_3 at elevated T (Xu et al., 2025), the fractional contributions of NO_3^- reached minimum in summer. Simultaneously, heightened photochemical processes during summer promote the secondary production of SO_4^{2-}. Moreover, most data points cluster near the vertex representing NH_4^+ in the ternary diagram (the corner where the molar fraction of NH_4^+ approaches 100 %). This directly indicates a relative abundance of NH_4^+ during the observation period. To further quantitatively validate this conclusion, we performed a linear fitting analysis between the predicted NH_4^+ and the observed NH_4^+, indicating that NH_4^+ remains in excess after neutralizing SO_4^{2-} and NO_3^- (Fig. S2). When assuming that NO_3^- and SO_4^{2-} exist in the forms of $(NH_4)_2SO_4$ and NH_4NO_3, the slope (k) for each season approaches 1, indicating complete conversion to $(NH_4)_2SO_4$ ($[NH_4^+] = [NO_3^-] \times 18/62 + [SO_4^{2-}] \times 36/96$, $\mu g\,m^{-3}$) rather than to acidic NH_4HSO_4 ($[NH_4^+] = [NO_3^-] \times 18/62 + [SO_4^{2-}] \times 18/96$). After SO_4^{2-} is completely neutralized, any excess NH_4^+ then reacts with NO_3^- to form NH_4NO_3. The $k < 1$ signifies the observed NH_4^+ concentration is higher than the NH_4^+ concentration predicted based on the complete neutralisation assumption,and NH_4^+ remains in excess after fully neutralising SO_4^{2-} and NO_3^-. In practice, the observed excess NH_4^+ may interact with other anions, such as Cl^- from biomass burning, potentially forming NH_4Cl (Ye et al., 2019). This demonstrates that NH_3 is sufficiently abundant in the Guanzhong Plain to fully neutralize the major inorganic acids. This provides direct chemical evidence explaining the elevated aerosol pH levels in the ammonia-rich Guanzhong Plain and establishes a foundation for the subsequent analysis of the buffering contribution of NH_x to aerosol acidity.

The concributions of the remaining ions (Cl^-, K^+, Mg^{2+}, Ca^{2+}, Na^+) were relatively low, collectively constituting 12.6 % of total WSIIs. The pronounced Ca^{2+} peak in spring,

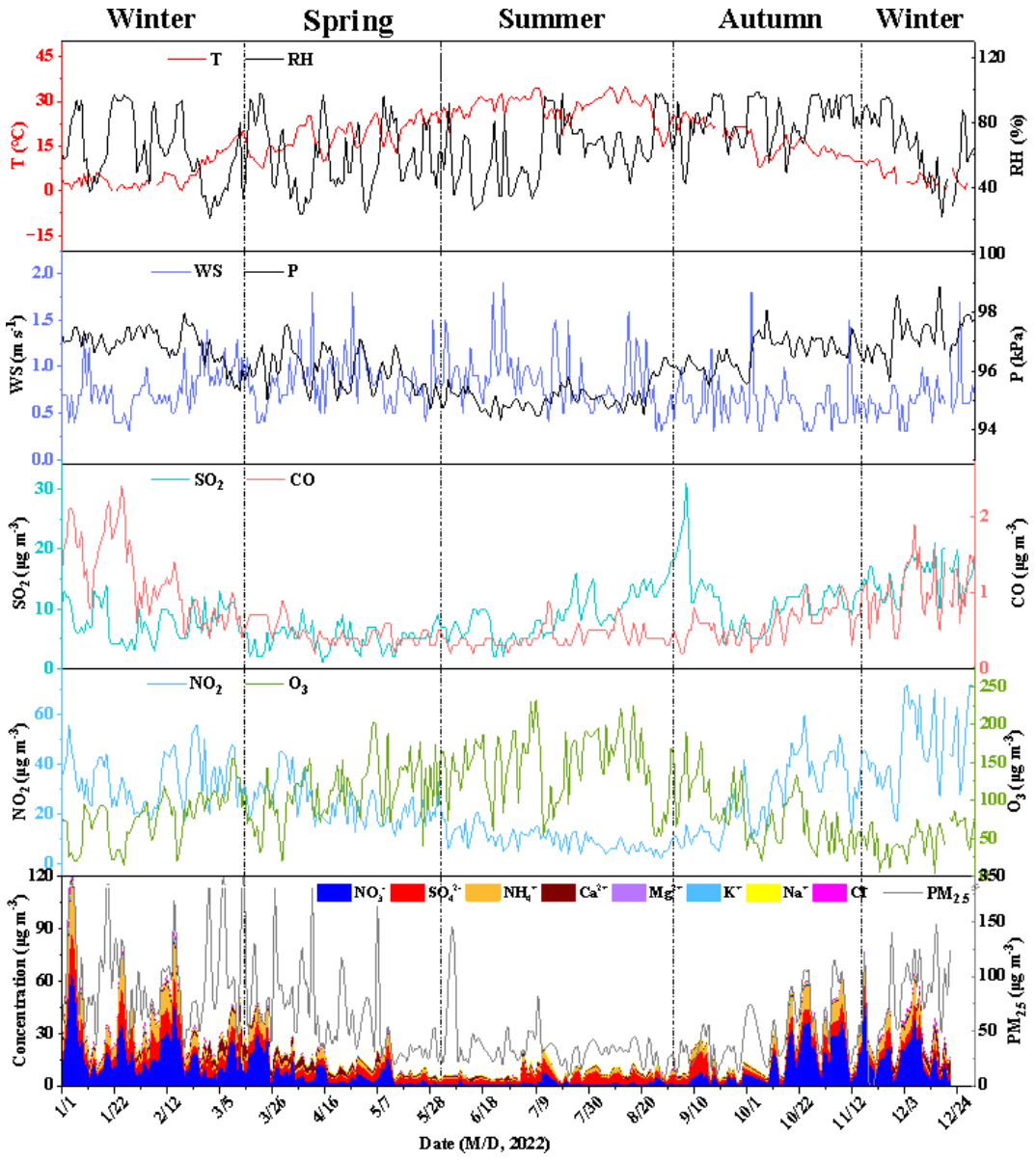

Figure 2. The time series data for $PM_{2.5}$ mass concentrations, criteria air pollutants (SO_2, CO, NO_2, and O_3-8 h), and meteorological parameters (T, RH, WS, and AP).

originating from dust transport from the Loess Plateau, introduces substantial alkaline mineral components into the atmosphere. These components provide an additional seasonal neutralization capacity and thus exert a significant influence on aerosol acidity (Shen et al., 2024). Cl^- and K^+, commonly utilized as tracers for anthropogenic combustion, exhibited highest concentration in winter, likely linked to seasonal biomass burning in western and northern China and subsequent regional transport processes (Liu et al., 2025a; Sun et al., 2013; Xie et al., 2020). These chemical characteristics, particularly the relative predominance of nitrate, reflect the evolution of $PM_{2.5}$ chemical properties influenced by China's air pollution control policies. Since the implementation of the Air Pollution Prevention and Control Action Plan in 2013, stringent industrial emission controls and coal reduction measures have yielded significant results, leading to a substantial decrease in SO_2 concentrations. Su et al. (2024) reported that SO_2 concentrations in Xi'an decreased by approximately 79 % from 2006 to 2021. This reduction has facilitated a shift in aerosol pollution type from sulfate-dominated to nitrate-dominated. This transformation in pollution type has emerged as a new characteristic of regional air pollution across China (Krotkov et al., 2016; Mao et al., 2022; Wang et al., 2022).

Table 2. Multiple linear regression results between NHR and its drivers (major particulate ions and meteorological factors) in each season.

Season	Prediction Equation	R	Sig.
Winter	$\mathrm{NHR} = 1.204 - 0.003\mathrm{SO_4^{2-}} + 0.006\mathrm{NO_3^-} + 0.023\mathrm{K^+} + 0.328\mathrm{Mg^{2+}} - 0.017\mathrm{Ca^{2+}} - 0.004T + 0.001\mathrm{RH}$	0.88	$P < 0.01$
Spring	$\mathrm{NHR} = 0.533 + 0.006\mathrm{SO_4^{2-}} + 0.005\mathrm{NO_3^-} - 0.018\mathrm{K^+} - 0.065\mathrm{Mg^{2+}} - 0.017\mathrm{Ca^{2+}} - 0.001T - 0.009\mathrm{RH}$	0.83	
Summer	$\mathrm{NHR} = -1.389 + 0.007\mathrm{SO_4^{2-}} + 0.006\mathrm{NO_3^-} + 0.01\mathrm{K^+} + 0.021\mathrm{Mg^{2+}} - 0.003\mathrm{Ca^{2+}} + 0.005T - 0.066\mathrm{RH}$	0.82	
Autumn	$\mathrm{NHR} = 0.656 + 0.006\mathrm{SO_4^{2-}} + 0.003\mathrm{NO_3^-} - 0.003\mathrm{K^+} + 0.064\mathrm{Mg^{2+}} - 0.040\mathrm{Ca^{2+}} - 0.001T + 0.012\mathrm{RH}$	0.86	

3.2 Establishment and validation of NH_3 concentration calculation methods

As a crucial precursor of secondary particulate matter, NH_3 influences aerosol acidity through the multiphase buffering of its NH_3/NH_4^+ conjugate pair (Liu et al., 2019; Saraswati et al., 2019; Zheng et al., 2020). This buffering effect is especially pronounced in the ammonia-rich Guanzhong Plain (Zhang et al., 2021c; Zheng et al., 2023). However, the lack of online monitoring data for gaseous NH_3 at the sampling site limits the accuracy of pH estimation using thermodynamic models. Therefore, it is important to establish a reliable method for estimating NH_3. In this study, we adapted the methodology of Wei et al. (2023) by replacing the prediction target from NH_3 to the thermodynamic state parameter NHR, and estimated the NHR using multiple linear regression analysis based on our previous short-term scale datasets (Wu et al., 2020). This is because the direct estimation of NH_3 is prone to interference from meteorological factors and the gas-particle distribution of acidic precursors, resulting in unstable outcomes in ammonia estimation. Consequently, this study opts to estimate NH_3 through NHR and assesses the method's accuracy (Meng et al., 2018; Wei et al., 2023).

Tables 2 and S4 summarize the total results of multiple linear regression analysis in each season. The F-test and t-test results reveal significant correlations for all seasons ($R > 0.82$, $P < 0.01$), confirming the efficacy of the established statistical regression equations. Subsequently, a Pearson correlation analysis was performed to elucidate the statistical associations between NHR and diverse environmental factors. As shown in Fig. 3 and Table S5, NHR exhibited significant correlations ($P < 0.01$) with all selected environmental factors in both winter and spring. Among these, the highest correlation coefficient was observed between NO_3^- and SO_4^{2-} ($R = 0.96$, $P < 0.01$). Across all four seasons, NHR showed good correlations with either NO_3^- or SO_4^{2-}, but with distinct seasonal variations. In winter and spring, NHR displayed the highest Pearson correlation coefficients with NO_3^- ($R = 0.86$, $P < 0.01$ in winter; $R = 0.74$, $P < 0.01$ in spring). Conversely, in summer and autumn, NHR correlated most significantly with SO_4^{2-} ($R = 0.75$, $P < 0.01$ in summer; $R = 0.79$, $P < 0.01$ in autumn). These seasonal distinctions primarily arise from fluctuations in the thermodynamic stability of different ammonium salts and the seasonal alterations in their formation pathways (Tao et al., 2025; Zhang et al., 2021c).

This study assessed the reliability of the MLR model estimates through two validation levels. First, the NHR estimated by the MLR model for 2016–2017 was compared to the observed NHR (Fig. 4). The results revealed a significant positive correlation across all seasons (with the intercept constrained to zero, $R^2 > 0.94$, $P < 0.01$), indicating that the MLR model predicts NHR with high accuracy. Second, to further validate the pH results at our site, we compared the NHR output from the ISORROPIA-II model with the input NHR (Fig. S3). The results again demonstrated a linear correlation (with the intercept constrained to zero, $R^2 > 0.83$, $P < 0.01$), thereby supporting the reliability of subsequent pH simulations. However, a disparity exists between the predicted and observed NHR in Figs. 4 and S3. To evaluate its impact on aerosol pH, we calculated the pH changes associated with both positive and negative NHR deviations (Table S1). The overall pH change resulting from these deviations is less than 0.2 units, which does not affect the primary conclusions. Furthermore, the NH_3 concentrations derived from NHR at our site remain below $60\,\mu g\,m^{-3}$, well within the range of the training dataset from urban site. However, the seasonal NH_3 pattern at our site (2022: winter > summer > spring > autumn) differs from that in the training dataset (2016: summer > spring > autumn > winter). This discrepancy can be attributed to the significant reduction in SO_2 emissions resulting from air pollution control. In 2016, the high concentration of SO_2 emitted from coal combustion reacts rapidly with NH_3 to form $(NH_4)_2SO_4$, and this process consumes large amounts of gaseous NH_3 in winter (Wang et al., 2016; Liu et al., 2023). Due to interannual NH_3 variability, we employed the thermodynamically stable NHR for model training and validation, back-calculated NH_3 from

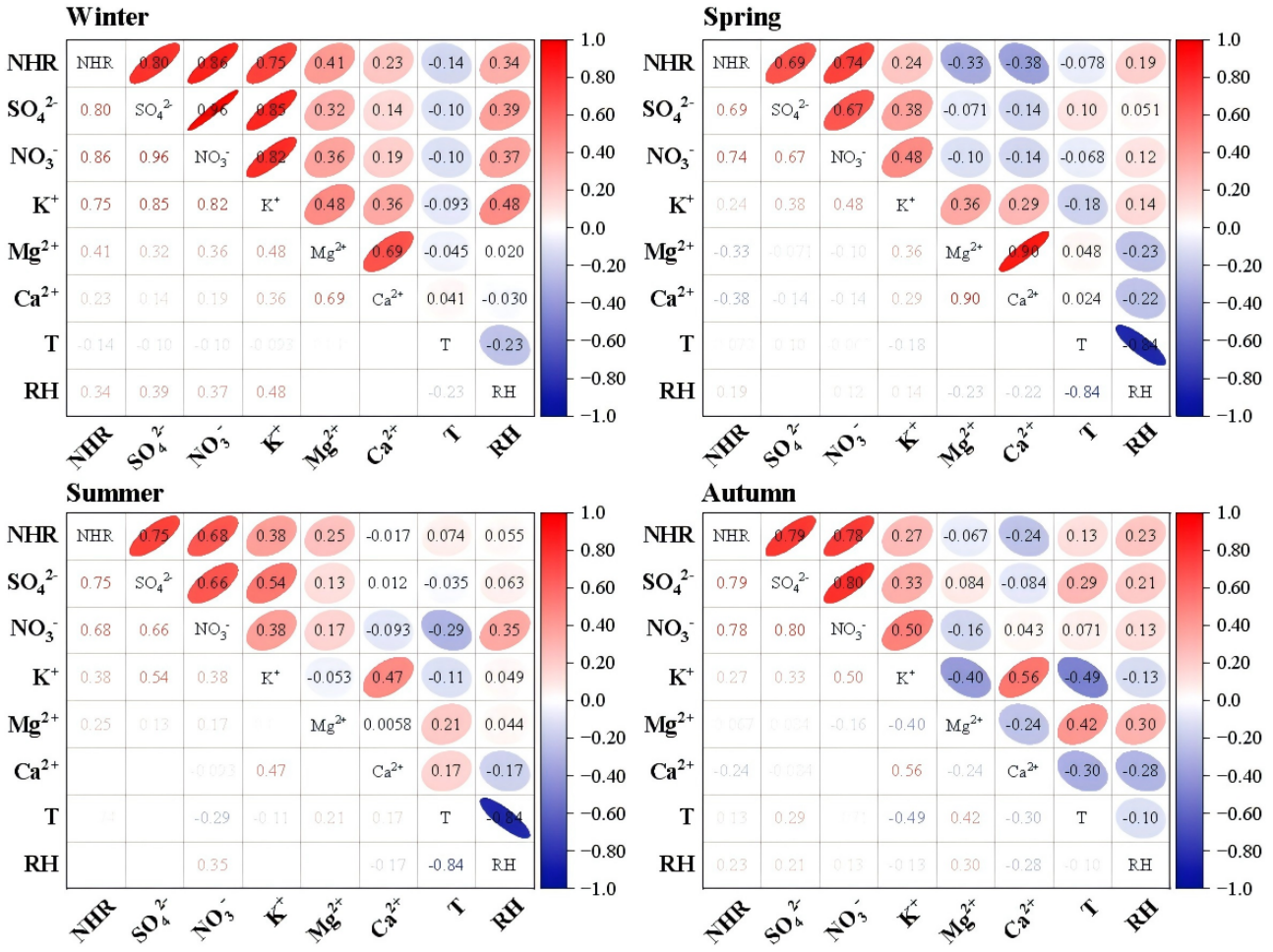

Figure 3. Pearson correlation among various factors.

the estimated NHR and measured NH_4^+, and then used these values in ISORROPIA-II to simulate aerosol pH.

3.3 Seasonal variation in aerosol pH and pH under different pollution levels

Figure 5 shows the monthly averages of aerosol pH, aerosol liquid water content (ALWC), and H^+_{air}, as calculated by the ISORROPIA-II model during the 2022 sampling period. The annual average aerosol pH at the Qinling observation site was 3.8 ± 1.0. The seasonal pH averages ranked as follows: winter (4.8 ± 0.5) > spring (3.6 ± 0.5) > autumn (3.3 ± 0.7) > summer (2.7 ± 0.7). The average ALWC concentration was $60.3\,\mu g\,m^{-3}$, exhibiting the pattern: winter ($80.4 \pm 112.9\,\mu g\,m^{-3}$) > autumn ($76.2 \pm 121.0\,\mu g\,m^{-3}$) > spring ($55.7 \pm 132.2\,\mu g\,m^{-3}$) > summer ($10.0 \pm 25.1\,\mu g\,m^{-3}$). Overall, aerosol pH was highest in winter and lowest in summer, with spring and autumn values intermediate. This trend closely aligns with the seasonal evolution of $PM_{2.5}$ chemical composition and meteorological conditions, reflecting the seasonal pH variation pattern observed in Beijing (Ding et al., 2019). Winter aerosol pH was similar to those reported in Xi'an previously and slightly higher than those recorded during the COVID-19 period (Liu et al., 2025b). A comparison of aerosol acidity levels across various regions in China is detailed in Table S6, revealing substantial regional variability. In contrast to southeastern coastal cities such as Shanghai and Xiamen, typical inland cities like Xi'an and Beijing generally display higher aerosol pH (Fu et al., 2022; Liu et al., 2025b; Xu et al., 2025).

To further explore the seasonal characteristics in $PM_{2.5}$ acidity/alkalinity under different pollution levels, this study classified $PM_{2.5}$ mass concentrations into two categories based on ambient air quality standards of China: clean days ($< 75\,\mu g\,m^{-3}$) and polluted days ($> 75\,\mu g\,m^{-3}$). A systematic comparison of percentage change in major WSIIs, aerosol pH and ALWC variations corresponding to these pollution levels across different seasons was performed (Table S7, Fig. S4). Under clean conditions, aerosol pH ranged from 2 to 5, whereas under polluted and heavily polluted conditions, it was primarily concentrated between 3 and 6. Inde-

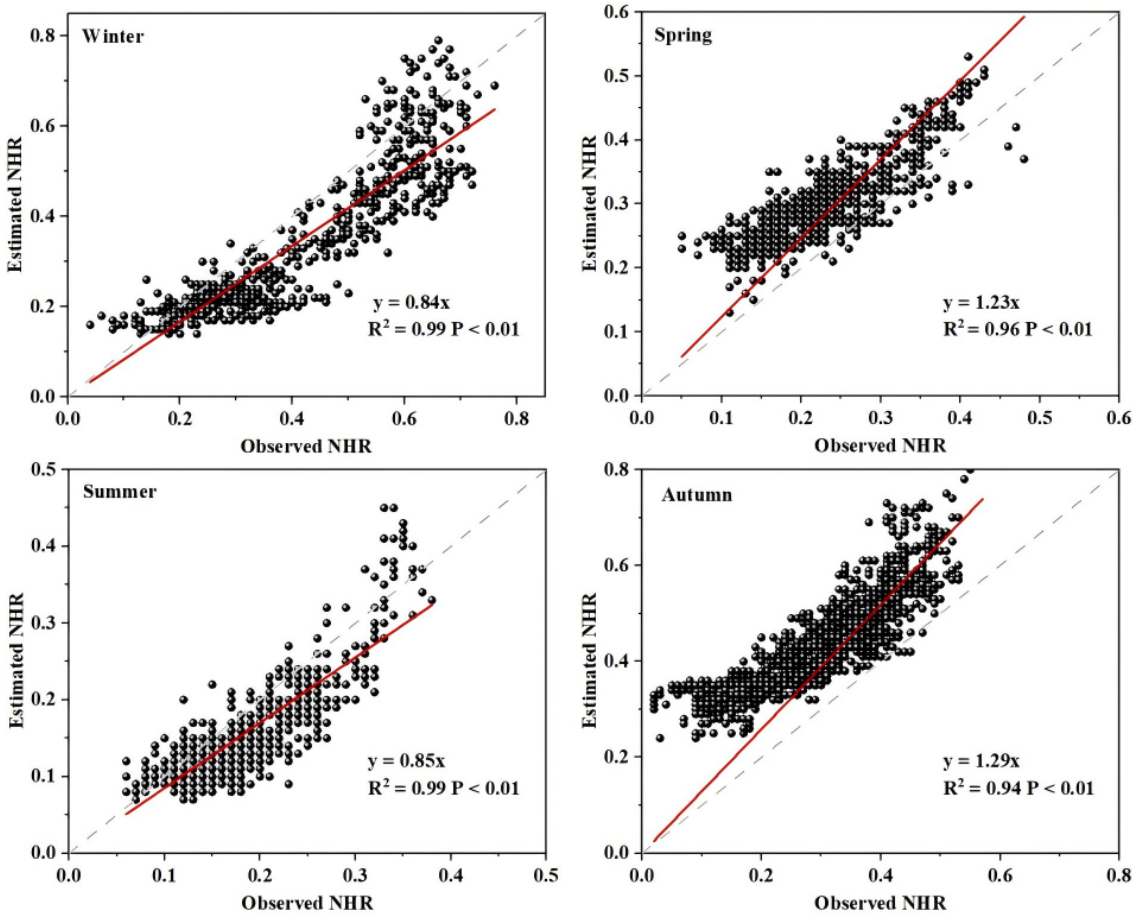

Figure 4. Correlation between hourly mean estimated and observed NHR in the training dataset.

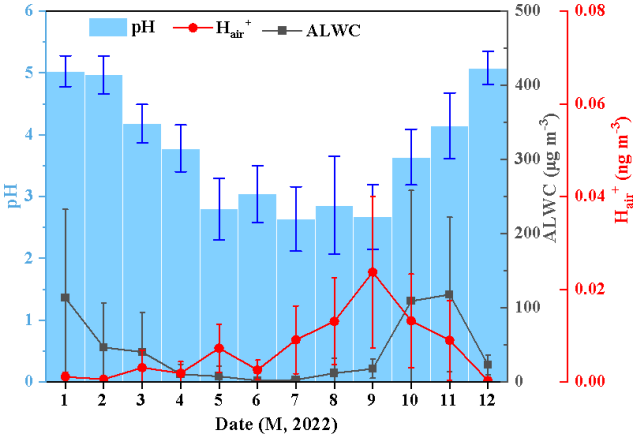

Figure 5. Monthly average aerosol pH, ALWC and H^+_{air} changes.

pendent *t*-tests confirmed significantly higher pH on polluted days for winter, spring, and autumn ($p < 0.01$). In summer, only two polluted days were recorded, so the statistical results for summer (Table S7) should be interpreted with caution due to the very limited sample size a reliable *t*-test could not be performed. As air quality declined and $PM_{2.5}$ concentrations increased from clean to polluted days, the concentrations of aerosol components and pH values exhibited an upward trend across all seasons. However, the behaviors of RH, ALWC, and H^+_{air} displayed seasonal discrepancies. In spring and summer, RH, ALWC, and H^+_{air} decreased as $PM_{2.5}$ concentrations increased. Conversely, during autumn and winter, these parameters increased alongside rising $PM_{2.5}$ concentrations. These findings reveal fundamental differences in the dominant chemical mechanisms of $PM_{2.5}$ pollution formation across seasons.

During spring and summer, pollution formation is mainly controlled by gas-phase photochemical oxidation (Chen et al., 2025; Li et al., 2021). The enhanced solar radiation and high temperatures during these seasons collectively create a highly oxidizing atmospheric environment. While promoting the transformation of precursors, these conditions also drive the decomposition of semi-volatile NH_4NO_3, leading to the release of gaseous HNO_3 and NH_3 (Guo et al., 2018; Tao et al., 2025). Consequently, despite an increase in $PM_{2.5}$ concentrations, both ALWC and H^+_{air} concentrations exhibit a decreasing or stabilizing trend due to the reduction of hy-

groscopic nitrate, while RH remains relatively low because of higher T. In contrast, autumn and winter are characterized by pollution processes driven by heterogeneous and aqueous-phase chemical reactions. The cold temperatures and stagnant weather conditions lead to high RH, promoting the aqueous-phase oxidation of pollutants and inhibiting the evaporation of NH_4NO_3 (Wang et al., 2016; Zhang et al., 2021c). This results in the significant formation of highly hygroscopic NH_4NO_3 and $(NH_4)_2SO_4$, which triggers an increase in ALWC. This increase further intensifies heterogeneous reactions and concentrates secondary acidic species such as H_2SO_4 and HNO_3, leading to a concurrent rise in H^+_{air} concentration. Consequently, a complex pollution scenario emerges, characterized by a simultaneous increase in $PM_{2.5}$ ALWC, and H^+_{air} concentrations.

3.4 Sensitivity analysis for aerosol pH

Sensitivity analysis of aerosol pH and ALWC in response to meteorological conditions and chemical composition is a crucial step for understanding and predicting atmospheric environmental changes. This analysis not only clarifies the nonlinear processes involved in secondary aerosol formation but also assesses the impact of variations in anthropogenic emissions on atmospheric chemical systems (Nah et al., 2023; Zhou et al., 2022). In this study, sensitivity analyses were performed for each season, incorporating both particulate-phase compositions and meteorological factors. The effects of SO_4^{2-}, NO_3^-, NH_x (gas NH_3 + NH_4^+), Cl^-, Ca^{2+}, K^+, Mg^{2+}, RH, and T on aerosol pH, ALWC, and H^+_{air} were evaluated, as illustrated in Fig. 6. The primary driving factors influencing aerosol pH variation across all seasons were NH_x, SO_4^{2-}, and T, while Ca^{2+} in spring and RH in summer also emerged as important influencing factors. This pattern is consistent with the driving factors identified in the Beijing area (Ding et al., 2019). Regarding ALWC, RH emerged as the most significant factor, followed by NO_3^- and SO_4^{2-}.

Sulfate as a key component of secondary inorganic aerosols, is one of the most significant acidic sources in atmospheric fine particulate matter. Sulfuric acid, generated through heterogeneous oxidation processes, is a strong acid that directly increases the concentration of H^+_{air} in the particulate phase and reduces the pH (Shah et al., 2018; Zhang et al., 2021c). As illustrated in Fig. 6, when the levels of alkaline substances such as NH_3 are maintained constant, aerosol pH significantly declines with increasing SO_4^{2-} concentration. The concurrent increase in ALWC and H^+_{air} confirms the sulfate-driven acidification mechanism: SO_2 is converted to H_2SO_4 via heterogeneous oxidation, and the dissociation of H_2SO_4 releases H^+, leading to increase H^+_{air} and decrease pH. (Ding et al., 2019). The increase in ALWC and H^+_{air} is particularly pronounced during summer and autumn. This sustained rise continuously depletes alkaline buffering substances in the particulate phase, resulting in increased acidity (Guo et al., 2018). Conversely, while nitrate similarly elevates H^+_{air} and ALWC, its overall impact on pH is generally weaker than that of sulfate due to its high volatility (Ding et al., 2019). Except during summer when the pH remained relatively stable, pH values decreased with rising NO_3^- concentrations in all other seasons.

Ammonia (NH_3), the primary alkaline gas, plays a crucial role in buffering aerosol pH. In ammonia-rich environments, NH_3 effectively counteracts acidic components, stabilizing pH and resulting in a nonlinear pH response to precursor concentrations (Cui et al., 2025; Karydis et al., 2021; Niu et al., 2016). Simultaneously, the dissolution of NH_3 into the particle phase to form NH_4^+ markedly enhances the hygroscopicity of particles, causing an increase in ALWC as NH_x concentrations rise (Jia et al., 2020; Liu et al., 2019). Studies indicate that NH_3 first reacts with H_2SO_4 and subsequently with HNO_3 to form NH_4NO_3. After most nitrate is converted to NH_4NO_3, it becomes difficult to dissolve additional NH_3 into aerosol droplets (Ding et al., 2019; Xu et al., 2025). The results of this study (Fig. 6) show that the response of pH to NH_x is non-linear. When the NH_x mass concentration is within the range of 3–10 $\mu g\,m^{-3}$, aerosol pH increases significantly, H^+_{air} decreases sharply, and ALWC increases with rising NH_x concentration. Nevertheless, when the NH_x concentration surpasses a specific threshold, the trends in pH and H^+_{air} decelerate and subsequently remain relatively stable. It should be noted that the results may be less accurate when NH_x concentration is below 3 $\mu g\,m^{-3}$, as high temperature and intense solar radiation promote the thermal decomposition of semi-volatile ammonium salts. The seasonal variations observed in this study further substantiate the regulatory role of atmospheric ammonia.

Ca^{2+} is an important crustal element in mineral dust, displaying distinct regional chemical characteristics and effects on aerosol acidity. According to the ISORROPIA-II model, Ca^{2+} typically combines with SO_4^{2-} to form the less soluble $CaSO_4$ solid phase, reducing its solubility and diminishing its effectiveness for neutralizing atmospheric acidity (Fountoukis and Nenes, 2007; Wang et al., 2016). In the Guanzhong Plain, the regulatory impact of Ca^{2+} on aerosol pH is particularly crucial, especially due to the region's proximity to the Loess Plateau and its semi-arid climate. Dust transport from the northwest could shape the alkaline atmospheric conditions in this area. This phenomenon results in neutral aerosol pH in the free troposphere and contributes to the alkalinity of cloud water at high-altitude sites (Liu et al., 2024; Shen et al., 2024). Elevated concentrations of Ca^{2+} can increase aerosol pH by decreasing both ALWC and H^+_{air}, with the most pronounced impact observed during the frequent dust events of spring. These events transport significant amounts of alkaline mineral dust, enhancing acid neutralization, consistent with studies in northern China (Shi et al., 2019; Tan et al., 2018). The relative standard deviation (RSD) can also be used to quantify the sensitivity of aerosol pH to a specific factor, with a higher RSD indicating a greater influence. This study revealed that RSD for Ca^{2+} concen-

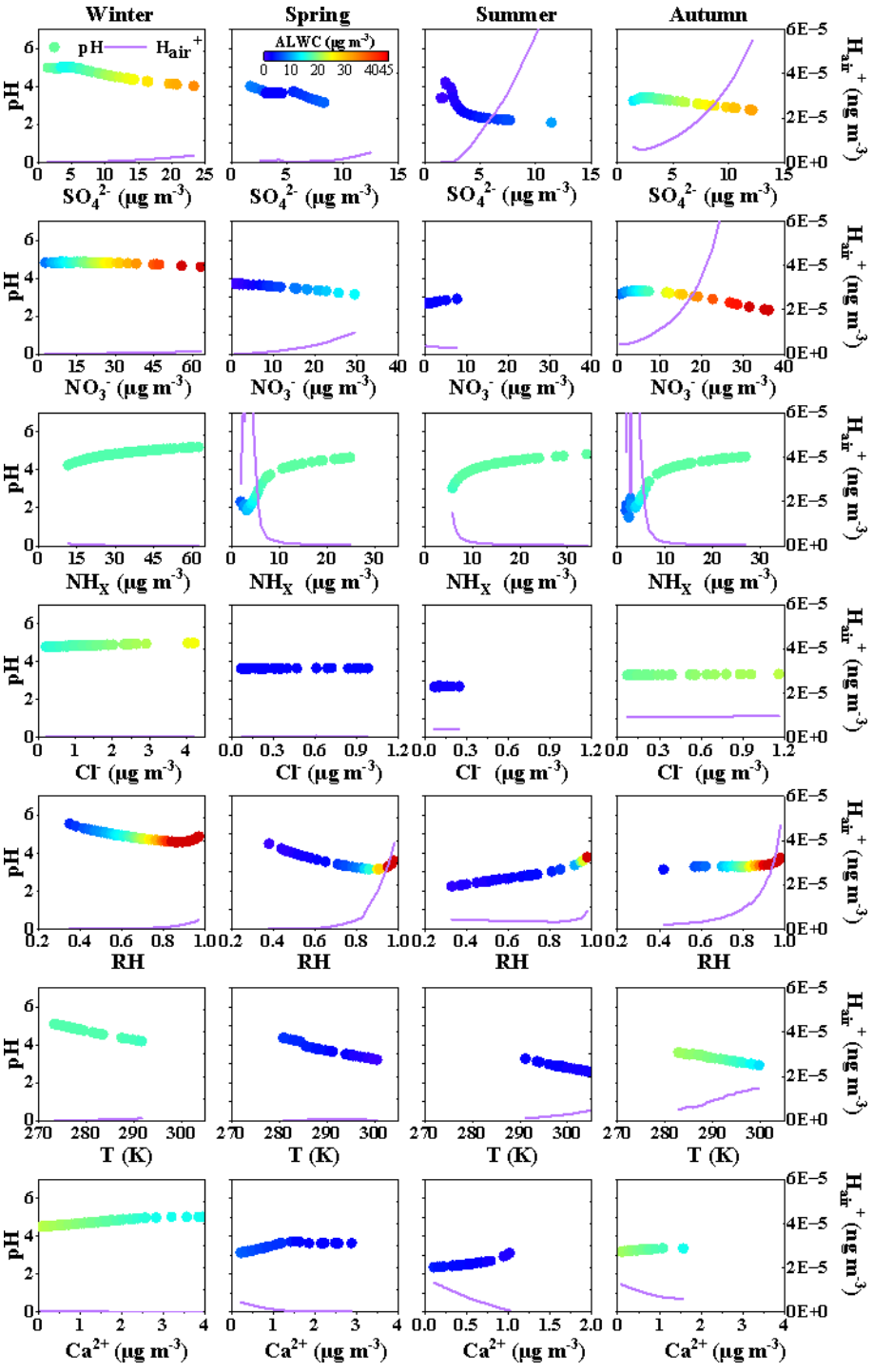

Figure 6. Sensitivity analysis of influencing factors.

tration variation in spring reached 8.8 % (Table S8), notably higher than the corresponding RSD of 7.5 % reported for the North China Plain during the same season (Ding et al., 2019). Conversely, in southern coastal urban areas like Xiamen and Guangzhou, which lack robust dust origins, the impact of Ca^{2+} on aerosol pH is typically negligible (Jia et al., 2020; Xu et al., 2025). This finding directly confirms the greater influence of dust sources in the Guanzhong Plain.

In addition to the particulate chemical composition, meteorological conditions, specifically RH and T, significantly influence aerosol acidity. This study revealed that during winter, spring, and autumn, aerosol pH displayed a non-

linear response to increasing RH, characterized by an initial decrease followed by a subsequent increase. The inflection point typically occurred within the RH range of 60 %–85 %. Beyond this critical threshold, ALWC entered a phase of exponential growth. This phenomenon is probably driven by the deliquescence of the predominant hygroscopic components within the aerosol, primarily NH_4NO_3 and $(NH_4)_2SO_4$, which have deliquescence relative humidities of approximately 62 % and 80 % (Tang, 1996). Notably, the inflection point exhibits clear seasonal variations, which can be attributed to seasonal shifts in aerosol chemical composition (Table 1). Notably, the inflection point varies seasonally maybe due to the varying proportions of NO_3^- and SO_4^{2-} in SNA: high NO_3^- in autumn and winter shifts the inflection point toward lower RH ($\sim$ 62 %), while the higher SO_4^{2-} contribution in spring shifts it toward higher RH ($\sim$ 80 %). Given that actual atmospheric particles are mixtures of various components, their hygroscopic and phase-state characteristics are more complicated (Su et al., 2022; Zheng et al., 2020). In the initial stage, an increase in RH results in a higher ALWC, which facilitates the heterogeneous uptake and aqueous-phase oxidation of acidic precursors, resulting in the formation of strong acids. During this phase, the acid-forming effect dominates the pH change (Du et al., 2020; Zhang et al., 2021c). Once RH exceeds a critical threshold, ALWC exhibits an exponential growth trend. At this point, the intense dilution effect of RH on H^+ begins to surpass the ongoing acid-forming effect (Karydis et al., 2021). Furthermore, this hygroscopic growth is self-reinforcing, i.e. the increased ALWC provides a more extensive aqueous medium for heterogeneous reactions of gaseous precursors, leading to further formation of hygroscopic salts and further promoting ALWC growth, and thus establishing a positive feedback loop (Su et al., 2022). Concurrently, under high RH conditions, thermodynamic factors favor the partitioning of semi-volatile ammonium salts into the particle phase. This neutralization process further depletes H^+ (Tao et al., 2025). These combined effects ultimately lead to the observed recovery in pH. Ambient temperature can influence aerosol pH by affecting gas-particle partitioning (Ding et al., 2019). The evaporation of semi-volatile ammonium salts plays a crucial role in aerosol acidification by transferring H^+ to the particle phase, consequently decreasing pH (Guo et al., 2018). Elevated ambient temperatures intensify this acidification mechanism synergistically. Thermodynamically, elevated temperatures drive the volatilization process. Concurrently, they reduce ALWC to concentrate H^+ and further enhance acidity.

3.5 Quantitative analysis of pH driving factors

To quantitatively analyze aerosol pH, the contributions of various influencing factors to aerosol pH and ALWC were further quantified (Figs. 7, S5; Table S2). According to the multiphase buffer theory (Zheng et al., 2020), T significantly drives the seasonal variation of aerosol pH by influencing pKa*. The results presented in Fig. 7 confirm this assertion, indicating that T plays a dominant role (22.3 %–31.6 %) in driving the seasonal variation of aerosol pH. T favored enhanced aerosol acidity in winter and spring, while the opposite trend was observed in summer and autumn. Moreover, NH_x emerged as a key factor influencing aerosol pH during winter and autumn, contributing between 22.9 % and 44.9 %. When the higher winter NH_x concentration (pH_1) was replaced with the lower concentration observed in spring (pH_2), while maintaining other winter parameters constant, the simulated $\Delta pH < 0$ ($pH_2 - pH_1$), indicating increased acidity. In the winter, the widespread use of coal for heating leads to significant emissions of acidic gases (Wang et al., 2016). The decrease in NH_3 concentrations may exacerbate acidification through two mechanisms. On one hand, lower NH_3 weakens the buffering capacity of the NH_3/NH_4^+ conjugate pair, which is the dominant alkaline buffer system for aerosol pH (Zheng et al., 2020). Less NH_3 is thus available to neutralize H^+ from SO_2 and NO_x oxidation, making the system more vulnerable to acidification. On the other hand, reduced NH_3 disturbs the gas-particle equilibrium between particulate ammonium nitrate and gaseous ammonia along with nitric acid. According to Le Chatelier's principle, a decrease in gas-phase NH_3 drives this equilibrium toward dissociation, promoting the decomposition of particulate NH_4NO_3 and releasing additional gaseous nitric acid (Guo et al., 2018). These two processes together contribute to a decline in system pH. In contrast, the opposite trend is observed in the autumn. The primary influencing factors in spring were T at 31.9 % and NVCs at 24.7 %, while in summer, they were T at 33.8 % and RH at 17.8 %. These results suggest that NVCs, represented by Ca^{2+}, are rich in alkaline mineral components and can enhance acid-neutralizing capacity, making them important drivers of aerosol pH variations in spring. In summer, RH alters aerosol acidity by affecting the deliquescence of hygroscopic particles, thereby serving as a key driver of aerosol pH variations. This observation is consistent with findings from studies conducted in other northern Chinese cities (Ding et al., 2019). Moreover, the combined effects of factor interactions and model nonlinearity, represented by the residual contribution (ΔpH_{others}) are also significant, particularly in autumn, where they contributed 26.6 % to aerosol pH variation.

Throughout the observation period, chemical components contributed an average of 47.7 % annually to pH, while meteorological factors contributed 35.7 %, highlighting the greater impact of chemical components over meteorological factors. This characteristic significantly differs from that observed in southeastern coastal regions of China. For example, studies conducted in Xiamen and Guangzhou have demonstrated that the contribution of meteorological factors frequently surpasses that of chemical components. This difference arises from regional characteristics. In coastal areas, meteorological factors, including RH and sea-land breezes, exhibit significant variability, while the chemical compo-

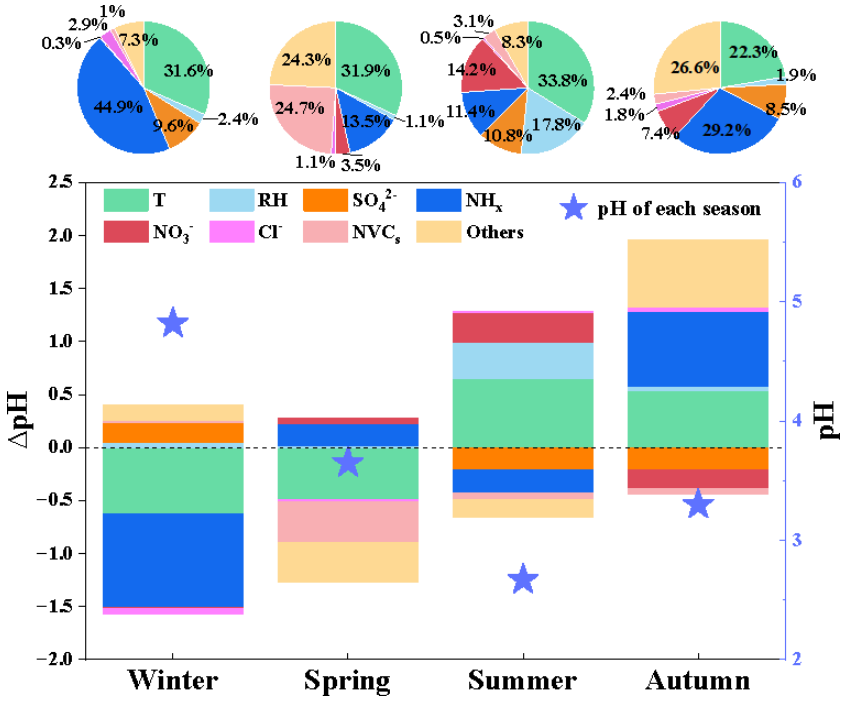

Figure 7. The contribution of various influencing factors to the seasonal pH. The asterisk represents the pH of aerosols in each season. The pie chart shows the relative contributions of various influencing factors to the seasonal pH (absolute values of pH was taken for pie chart).

sition remains relatively stable, rendering meteorological conditions predominant. Conversely, in inland semi-arid regions, chemical components such as NH_x and dust-derived Ca^{2+} exhibit pronounced seasonal fluctuations, resulting in a greater dominance of chemical factors (Jia et al., 2020; Xu et al., 2025). Seasonally, chemical components were more influential in winter (58.7 %), spring (42.7 %), and autumn (49.2 %). Conversely, meteorological factors displayed their most significant impact in summer, with a contribution rate reaching 51.6 %, thus serving as the primary driver of pH variation during this season.

4 Conclusions

This study evaluates the aerosol acidity across four seasons in the Guanzhong region of China and quantitatively analyzes the factors contributing to seasonal pH variations. Over the study period, $PM_{2.5}$ in the study area was generally weakly alkaline, with an annual mean aerosol pH of 3.8 ± 1.0. This trend corresponds with the seasonal changes in $PM_{2.5}$ chemical composition and meteorological conditions. Aerosol pH increased alongside rising $PM_{2.5}$ concentrations, ranging from 2–5 (average: 3.4 ± 0.9) on clean days to 3–6 (4.8 ± 0.5) on polluted and heavily polluted days. Sensitivity analysis and quantitative analysis indicated that NH_x, SO_4^{2-}, RH, and T are key drivers driving pH across all seasons. T emerged as the primary driver of seasonal pH fluctuations (contributing 22.3 %–31.6 %), with NH_x playing a significant role in autumn and winter (contributing 22.9 %–44.9 %), while Ca^{2+} in spring and RH in summer acted as specific driving factor for those seasons. pH showed higher sensitivity to SO_4^{2-} than to NO_3^-. Furthermore, NH_x not only displayed substantial buffering capacity on pH but also, upon conversion to NH_4^+ in the particle phase, enhanced particle hygroscopicity, resulting in increased ALWC with higher NH_x concentrations. Meteorological conditions, beyond chemical components, exerted a non-linear regulatory influence on acidity. During winter, spring, and autumn, aerosol pH initially decreases and subsequently increases with rising RH, exhibiting an inflection point within the RH range of 60 %–85 %. This behavior might be related to the explosive growth in ALWC that occurs when the predominant hygroscopic components, primarily NH_4NO_3 and $(NH_4)_2SO_4$, reach their mixed deliquescence point. Our results discovered the main driving factors of aerosol acidity and alkalinity in the Guanzhong Plain, which would be helpful for deeply understanding the heterogenous formation of atmospheric secondary aerosols in the semi-arid region.

Data availability. The data in this study are available at https://doi.org/10.5281/zenodo.18455742 (Wang et al., 2026).

Supplement. The supplement related to this article is available online at https://doi.org/10.5194/acp-26-11785-2026-supplement.

Author contributions. Jianjun Li conceived and designed the study, and the revision of the manuscript. Qian Wang conducted the literature search, performed sample and data analysis, and wrote the manuscript. Xiao Guo, Minxia Shen, Yali Liu, Yifan Zhang, Lu Li, Weining Qi, Yue Cao, Shicong Li, Zhuoer Dong and Wenting Dai collected particulate samples and supervised the experiments. All authors provided critical feedback on the manuscript and approved the final version.

Competing interests. The contact author has declared that none of the authors has any competing interests.

Disclaimer. Publisher's note: Copernicus Publications remains neutral with regard to jurisdictional claims made in the text, published maps, institutional affiliations, or any other geographical representation in this paper. The authors bear the ultimate responsibility for providing appropriate place names. Views expressed in the text are those of the authors and do not necessarily reflect the views of the publisher.

Acknowledgements. This work was supported by the program from National Natural Science Foundation of China (No. 42577120), the Natural Science Basic Research Program of Shaanxi (2025JC-YBQN-450) and the National Natural Science Foundation of China (No. 42407156). Jianjun Li also acknowledged the support of the Youth Innovation Promotion Association Chinese Academy of Sciences.

Financial support. This research has been supported by the National Natural Science Foundation of China (grant no. 42577120), the Natural Science Basic Research Program of Shaanxi Province (grant no. 2025JC-YBQN-450), and the National Natural Science Foundation of China (grant no. 42407156).

Review statement. This paper was edited by Benjamin A Nault and reviewed by four anonymous referees.

References

Brook, R., Wiebe, A. H., Woodhouse, A., Audette, V., Piechowski, M., Dabek-Zlotorzynska, E., and Dloughy, F.: Temporal and spatial relationships in fine particle strong acidity, sulphate, PM_{10}, and $PM_{2.5}$ across multiple Canadian locations, Atmos. Environ., 31, 4223–4236, https://doi.org/10.1016/S1352-2310(97)00248-3, 1997.

Chen, G., Fan, X., Lin, Z., Ji, X., Chen, Z., Xu, L., and Chen, J.: Driving factors and photochemical impacts of Cl_2 in coastal atmosphere of southeast China, npj Clim. Atmos. Sci., 8, 135, https://doi.org/10.1038/s41612-025-01022-y, 2025.

Clegg, S. L., Brimblecombe, P., and Wexler, A. S.: Thermodynamic model of the system H^+-NH_4^+-Na^+-SO_4^{2-}-NO_3^--Cl^--H_2O at 298.15 K, J. Phys. Chem. A, 102, 2155–2171, https://doi.org/10.1021/jp973043j, 1998.

Cui, H., Du, Y., Zhang, H., Deng, M., Zhang, Q., Chen, W., Su, S., Li, X., Sarkar, S., Yang, L., Wang, X., and Jia, S.: A quantitative study on the influencing pathways of aerosol acidity: the non-neglectable role of non-ideality, Atmos. Environ., 354, 121256, https://doi.org/10.1016/j.atmosenv.2025.121256, 2025.

Ding, J., Zhao, P., Su, J., Dong, Q., Du, X., and Zhang, Y.: Aerosol pH and its driving factors in Beijing, Atmos. Chem. Phys., 19, 7939–7954, https://doi.org/10.5194/acp-19-7939-2019, 2019.

Du, C., Yang, H., Wang, N., Pang, S., and Zhang, Y.: pH effect on the release of NH_3 from the internally mixed sodium succinate and ammonium sulfate aerosols, Atmos. Environ., 220, 117101, https://doi.org/10.1016/j.atmosenv.2019.117101, 2020.

Feng, Q., Liu, H., Dai, W., Cao, Y., Shen, M., Liu, Y., Qi, W., Chen, Y., Guo, X., Zhang, Y., Li, L., Zhou, B., and Li, J.: Comparison of chemical composition and acidity of size-resolved inorganic aerosols at the top and foot of mt. Hua, northwest China: the role of the gas-particle distribution of ammonia, Sci. Total Environ., 905, 166985, https://doi.org/10.1016/j.scitotenv.2023.166985, 2023.

Fountoukis, C. and Nenes, A.: ISORROPIA II: a computationally efficient thermodynamic equilibrium model for K^+–Ca^{2+}–Mg^{2+}–NH_4^+–Na^+–SO_4^{2-}–NO_3^-––Cl^-–H_2O aerosols, Atmos. Chem. Phys., 7, 4639–4659, https://doi.org/10.5194/acp-7-4639-2007, 2007.

Fu, Z., Cheng, L., Ye, X., Ma, Z., Wang, R., Duan, Y., Tao, J., and Cheng, J.: Characteristics of aerosol chemistry and acidity in shanghai after $PM_{2.5}$ satisfied national guideline: Insight into future emission control, Sci. Total Environ., 827, 154319, https://doi.org/10.1016/j.scitotenv.2022.154319, 2022.

Guo, H., Xu, L., Bougiatioti, A., Cerully, K. M., Capps, S. L., Hite Jr., J. R., Carlton, A. G., Lee, S.-H., Bergin, M. H., Ng, N. L., Nenes, A., and Weber, R. J.: Fine-particle water and pH in the southeastern United States, Atmos. Chem. Phys., 15, 5211–5228, https://doi.org/10.5194/acp-15-5211-2015, 2015.

Guo, H., Sullivan, A. P., Campuzano-Jost, P., Schroder, J. C., Lopez-Hilfiker, F. D., Dibb, J. E., Jimenez, J. L., Thornton, J. A., Brown, S. S., Nenes, A., and Weber, R. J.: Fine particle pH and the partitioning of nitric acid during winter in the northeastern united states, J. Geophys. Res.-Atmos., 121, https://doi.org/10.1002/2016JD025311, 2016.

Guo, H., Otjes, R., Schlag, P., Kiendler-Scharr, A., Nenes, A., and Weber, R. J.: Effectiveness of ammonia reduction on control of fine particle nitrate, Atmos. Chem. Phys., 18, 12241–12256, https://doi.org/10.5194/acp-18-12241-2018, 2018.

Hennigan, C. J., Izumi, J., Sullivan, A. P., Weber, R. J., and Nenes, A.: A critical evaluation of proxy methods used to estimate the acidity of atmospheric particles, Atmos. Chem. Phys., 15, 2775–2790, https://doi.org/10.5194/acp-15-2775-2015, 2015.

Huang, R., Zhang, Y., Bozzetti, C., Ho, K., Cao, J., Han, Y., Daellenbach, K. R., Slowik, J. G., Platt, S. M., Canonaco, F., Zotter, P., Wolf, R., Pieber, S. M., Bruns, E. A., Crippa, M., Ciarelli, G., Piazzalunga, A., Schwikowski, M., Abbaszade, G., Schnelle-Kreis, J., Zimmermann, R., An, Z., Szidat, S., Baltensperger, U., Haddad, I. E., and Prévôt, A. S. H.: High secondary aerosol contribution to particulate pollution during haze events in China, Nature, 514, 218–222, https://doi.org/10.1038/nature13774, 2014.

Jia, S., Chen, W., Zhang, Q., Krishnan, P., Mao, J., Zhong, B., Huang, M., Fan, Q., Zhang, J., Chang, M., Yang, L., and Wang, X.: A quantitative analysis of the driv-

ing factors affecting seasonal variation of aerosol pH in Guangzhou, China, Sci. Total Environ., 725, 138228, https://doi.org/10.1016/j.scitotenv.2020.138228, 2020.

Karydis, V. A., Tsimpidi, A. P., Pozzer, A., and Lelieveld, J.: How alkaline compounds control atmospheric aerosol particle acidity, Atmos. Chem. Phys., 21, 14983–15001, https://doi.org/10.5194/acp-21-14983-2021, 2021.

Krotkov, N. A., McLinden, C. A., Li, C., Lamsal, L. N., Celarier, E. A., Marchenko, S. V., Swartz, W. H., Bucsela, E. J., Joiner, J., Duncan, B. N., Boersma, K. F., Veefkind, J. P., Levelt, P. F., Fioletov, V. E., Dickerson, R. R., He, H., Lu, Z., and Streets, D. G.: Aura OMI observations of regional SO_2 and NO_2 pollution changes from 2005 to 2015, Atmos. Chem. Phys., 16, 4605–4629, https://doi.org/10.5194/acp-16-4605-2016, 2016.

Li, K., Jacob, D. J., Liao, H., Qiu, Y., Shen, L., Zhai, S., Bates, K. H., Sulprizio, M. P., Song, S., Lu, X., Zhang, Q., Zheng, B., Zhang, Y., Zhang, J., Lee, H. C., and Kuk, S. K.: Ozone pollution in the north China plain spreading into the late-winter haze season, P. Natl. Acad. Sci. USA, 118, e2015797118, https://doi.org/10.1073/pnas.2015797118, 2021.

Liu, H., Feng, Q., Huang, Y., Wu, F., Liu, Y., Shen, M., Guo, X., Dai, W., Qi, W., Zhang, Y., Li, L., Wang, Q., Zhou, B., and Li, J.: Composition and size distribution of wintertime inorganic aerosols at ground and alpine regions of northwest China, Chinese Chem. Lett., 35, 109636, https://doi.org/10.1016/j.cclet.2024.109636, 2024.

Liu, M., Song, Y., Zhou, T., Xu, Z., Yan, C., Zheng, M., Wu, Z., Hu, M., Wu, Y., and Zhu, T.: Fine particle pH during severe haze episodes in northern China, Geophys. Res. Lett., 44, 5213–5221, https://doi.org/10.1002/2017GL073210, 2017.

Liu, M., Huang, X., Song, Y., Tang, J., Cao, J., Zhang, X., Zhang, Q., Wang, S., Xu, T., Kang, L., Cai, X., Zhang, H., Yang, F., Wang, H., Yu, J. Z., Lau, A. K., He, L., Huang, X., Duan, L., Ding, A., Xue, L., Gao, J., Liu, B., and Zhu, T.: Ammonia emission control in China would mitigate haze pollution and nitrogen deposition, but worsen acid rain, P. Natl. Acad. Sci. USA, 116, 7760–7765, https://doi.org/10.1073/pnas.1814880116, 2019.

Liu, M., Liu, Z., Wang, J., Chen, W., Feng, T., Pan, T., Yuan, B., Huang, S., Shao, M., Hu, M., Wang, X., and Hu, W.: The variation, source, and environmental impact of chloride across China: summarized field results based on the aerosol mass spectrometer (AMS), J. Geophys. Res.-Atmos., 130, e2024JD043275, https://doi.org/10.1029/2024JD043275, 2025a.

Liu, P., Zhao, X., Zhang, C., Chen, H., Wang, J., Xue, L., Chen, J., and Mu, Y.: Fine particle pH and its influencing factors during summer at Mt. Tai: comparison between mountain and urban sites, Atmos. Environ., 261, 118607, https://doi.org/10.1016/j.atmosenv.2021.118607, 2021.

Liu, P., Chen, H., Song, Y., Xue, C., Ye, C., Zhao, X., Zhang, C., Liu, J., and Mu, Y.: Atmospheric ammonia in the rural North China Plain during wintertime: Variations, sources, and implications for HONO heterogeneous formation, Sci. Total Environ., 861, 160768, https://doi.org/10.1016/j.scitotenv.2022.160768, 2023.

Liu, Y., Guo, X., Zhang, Y., Cao, Y., Jiang, Y., Qi, W., Shen, M., Li, L., Wang, Q., Dai, W., and Li, J.: Chemical characteristics of wintertime $PM_{2.5}$ in background region of northwest China during urban emission reduction, Iscience, 28, 113528, https://doi.org/10.1016/j.isci.2025.113528, 2025b.

Mao, I., Lin, C, Lin, C., Chen, Y., Sung, F., and Chen, M.: Exposure of acid aerosol for schoolchildren in metropolitan Taipei, Atmos. Environ., 43, 5622–5629, https://doi.org/10.1016/j.atmosenv.2009.07.054, 2009.

Mao, M., Rao, L., Jiang, H., He, S., and Zhang, X.: Air pollutants in metropolises of eastern coastal China, Int. J. Env. Res. Pub. He., 19, 15332, https://doi.org/10.3390/ijerph192215332, 2022.

Meng, Z., Xu, X., Lin, W., Ge, B., Xie, Y., Song, B., Jia, S., Zhang, R., Peng, W., Wang, Y., Cheng, H., Yang, W., and Zhao, H.: Role of ambient ammonia in particulate ammonium formation at a rural site in the North China Plain, Atmos. Chem. Phys., 18, 167–184, https://doi.org/10.5194/acp-18-167-2018, 2018.

Nah, T., Lam, Y. H., Yang, J., and Yang, L.: Long-term trends and sensitivities of $PM_{2.5}$ pH and aerosol liquid water to chemical composition changes and meteorological parameters in Hong Kong, south China: insights from 10-year records from three urban sites, Atmos. Environ., 302, 119725, https://doi.org/10.1016/j.atmosenv.2023.119725, 2023.

Nenes, A., Pandis, S. N., and Pilinis, C.: ISORROPIA: A new thermodynamic equilibrium model for multiphase multicomponent inorganic aerosols, Aquat. Geochem., 4, 123–152, https://doi.org/10.1023/A:1009604003981, 1998.

Niu, X., Cao, J., Shen, Z., Ho, S. S. H., Tie, X., Zhao, S., Xu, H., Zhang, T., and Huang, R.: $PM_{2.5}$ from the Guanzhong Plain: chemical composition and implications for emission reductions, Atmos. Environ., 147, 458–469, https://doi.org/10.1016/j.atmosenv.2016.10.029, 2016.

Paglione, M., Decesari, S., Rinaldi, M., Tarozzi, L., Manarini, F., Gilardoni, S., Facchini, M. C., Fuzzi, S., Bacco, D., Trentini, A., Pandis, S. N., and Nenes, A.: Historical changes in seasonal aerosol acidity in the po valley (Italy) as inferred from fog water and aerosol measurements, Environ. Sci. Technol., 55, 7307–7315, https://doi.org/10.1021/acs.est.1c00651, 2021.

Pye, H. O. T., Nenes, A., Alexander, B., Ault, A. P., Barth, M. C., Clegg, S. L., Collett Jr., J. L., Fahey, K. M., Hennigan, C. J., Herrmann, H., Kanakidou, M., Kelly, J. T., Ku, I.-T., McNeill, V. F., Riemer, N., Schaefer, T., Shi, G., Tilgner, A., Walker, J. T., Wang, T., Weber, R., Xing, J., Zaveri, R. A., and Zuend, A.: The acidity of atmospheric particles and clouds, Atmos. Chem. Phys., 20, 4809–4888, https://doi.org/10.5194/acp-20-4809-2020, 2020.

Rengarajan, R., Sudheer, A., and Sarin, M.: Aerosol acidity and secondary organic aerosol formation during wintertime over urban environment in western India, Atmos. Environ., 45, 1940–1945, https://doi.org/10.1016/j.atmosenv.2011.01.026, 2011.

Saraswati, Sharma, S., Saxena, M., and Mandal, T.: Characteristics of gaseous and particulate ammonia and their role in the formation of secondary inorganic particulate matter at Delhi, India, Atmos. Res., 218, 34–49, https://doi.org/10.1016/j.atmosres.2018.11.010, 2019.

Shah, V., Jaeglé, L., Thornton, J., Lopez-Hilfiker, F., Lee, B., Schroder, J., Campuzano-Jost, P., Jimenez, J., Guo, H., Sullivan, A., Weber, R., Green, J., Fiddler, M., Bililign, S., Campos, T., Stell, M., Weinheimer, A., Montzka, D., and Brown, S.: Chemical feedbacks weaken the wintertime response of particulate sulfate and nitrate to emissions reductions over the eastern United States, P. Natl. Acad. Sci. USA, 115, 8110–8115, https://doi.org/10.1073/pnas.1803295115, 2018.

Shen, M., Li, J., Liu, Y., Dai, W., Wang, G., Qi, W., Chen, Y., Guo, X., Zhang, Y., Li, L., Cao, Y., Feng, Q., Su, H.,

and Cao, J.: Comparison of acidity and chemical composition of summertime cloud water and aerosol at an alpine site in northwest China: Implications for the neutral property of clouds in the free troposphere, Sci. Total Environ., 925, 171775, https://doi.org/10.1016/j.scitotenv.2024.171775, 2024.

Shi, G., Xu, J., Shi, X., Liu, B., Bi, X., Xiao, Z., Chen, K., Wen, J., Dong, S., Tian, Y., Feng, Y., Yu, H., Song, S., Zhao, Q., Gao, J., and Russell, A. G.: Aerosol pH dynamics during haze periods in an urban environment in China: use of detailed, hourly, speciated observations to study the role of ammonia availability and secondary aerosol formation and urban environment, J. Geophys. Res.-Atmos., 124, 9730–9742, https://doi.org/10.1029/2018JD029976, 2019.

Shi, Z., Bonneville, S., Krom, M. D., Carslaw, K. S., Jickells, T. D., Baker, A. R., and Benning, L. G.: Iron dissolution kinetics of mineral dust at low pH during simulated atmospheric processing, Atmos. Chem. Phys., 11, 995–1007, https://doi.org/10.5194/acp-11-995-2011, 2011.

Song, S., Nenes, A., Gao, M., Zhang, Y., Liu, P., Shao, J., Ye, D., Xu, W., Sun, Y., Liu, B., and McElroy, M.: Thermodynamic Modeling Suggests Declines in Water Uptake and Acidity of Inorganic Aerosols in Beijing Winter Haze Events during 2014/2015–2018/2019, Environ. Sci. Technol., 6, 752–760, https://doi.org/10.1021/acs.estlett.9b00621, 2019.

Su, H., Zhang, T., Liu, S., Qu, Y., Li, H., Zhou, J., Zhao, Z., Wang, Q., Li, L., Shen, M., and Chen, S.: Growth of nitrate contribution to aerosol pollution during wintertime in Xi'an, northwest China: Formation mechanism and effects of NH_3, Particuology, 87, 303–315, https://doi.org/10.1016/j.partic.2023.09.014, 2024.

Su, J., Zhao, P., Ge, S., and Ding, J.: Aerosol liquid water content of $PM_{2.5}$ and its influencing factors in Beijing, China, Sci. Total Environ., 839, 156342, https://doi.org/10.1016/j.scitotenv.2022.156342, 2022.

Sun, Y. L., Wang, Z. F., Fu, P. Q., Yang, T., Jiang, Q., Dong, H. B., Li, J., and Jia, J. J.: Aerosol composition, sources and processes during wintertime in Beijing, China, Atmos. Chem. Phys., 13, 4577–4592, https://doi.org/10.5194/acp-13-4577-2013, 2013.

Tan, T., Hu, M., Li, M., Guo, Q., Wu, Y., Fang, X., Gu, F., Wang, Y., and Wu, Z.: New insight into $PM_{2.5}$ pollution patterns in Beijing based on one-year measurement of chemical compositions, Sci. Total Environ., 621, 734–743, https://doi.org/10.1016/j.scitotenv.2017.11.208, 2018.

Tang, I.: Chemical and size effects of hygroscopic aerosols on light scattering coefficients. J. Geophys. Res.-Atmos., 101, 19245–19250, https://doi.org/10.1029/96JD03003, 1996.

Tao, J., Wu, Y., Deng, Y., Hu, B., and Zhou, Z.: Thermodynamic regulation of aerosol pH by temperature and humidity: the role of gas-particle partitioning of semi-volatile inorganic species in a subtropical region, Environ. Res., 286, 122727, https://doi.org/10.1016/j.envres.2025.122727, 2025.

Tao, Y. and Murphy, J. G.: The sensitivity of PM2.5 acidity to meteorological parameters and chemical composition changes: 10-year records from six Canadian monitoring sites, Atmos. Chem. Phys., 19, 9309–9320, https://doi.org/10.5194/acp-19-9309-2019, 2019.

Wang, G., Zhang, R., Gomez, M., Yang, L., Levy Zamora, M., Hu, M., Lin, Y., Peng, J., Guo, S., Meng, J., Li, J., Cheng, C., Hu, T., Ren, Y., Wang, Y., Gao, J., Cao, J., An, Z., Zhou, W., Li, G., Wang, J., Tian, P., Marrero-Ortiz, W., Secrest, J., Du, Z., Zheng, J., Shang, D., Zeng, L., Shao, M., Wang, W., Huang, Y., Wang, Y., Zhu, Y., Li, Y., Hu, J., Pan, B., Cai, L., Cheng, Y., Ji, Y., Zhang, F., Rosenfeld, D., Liss, P., Duce, R., Kolb, C., and Molina, M.: Persistent sulfate formation from London fog to Chinese haze, P. Natl. Acad. Sci. USA, 113, 13630–13635, https://doi.org/10.1073/pnas.1616540113, 2016.

Wang, Q., Guo, Xiao., Shen, M., Liu, Y., Zhang, Y., Li, L., Qi, W., Cao, Y., Li, S., Dong, Z., and Dai, W.: Measurement report: quantitative analysis of aerosol acidity and its driving factors in guanzhong area, northwest China, Zenodo [data set], https://doi.org/10.5281/zenodo.18455742, 2026.

Wang, Z., Wang, R., Wang, J., Wang, Y., McPherson Donahue, N., Tang, R., Dong, Z., Li, X., Wang, L., Han, Y., and Cao, J.: The seasonal variation, characteristics and secondary generation of $PM_{2.5}$ in Xi'an, China, especially during pollution events, Environ. Res., 212, 113388, https://doi.org/10.1016/j.envres.2022.113388, 2022.

Wei, Y., Wang, S., Jiang, N., Zhang, R., and Hao, Q.: Comparative multi-model study of $PM_{2.5}$ acidity trend changes in ammonia-rich regions in winter: based on a new ammonia concentration assessment method, J. Hazard. Mater., 458, 131970, https://doi.org/10.1016/j.jhazmat.2023.131970, 2023.

Wu, C., Wang, G., Li, J., Li, J., Cao, C., Ge, S., Xie, Y., Chen, J., Li, X., Xue, G., Wang, X., Zhao, Z., and Cao, F.: The characteristics of atmospheric brown carbon in Xi'an, inland China: sources, size distributions and optical properties, Atmos. Chem. Phys., 20, 2017–2030, https://doi.org/10.5194/acp-20-2017-2020, 2020.

Xie, Y., Lu, H., Yi, A., Zhang, Z., Zheng, N., Fang, X., and Xiao, H.: Characterization and source analysis of water–soluble ions in $PM_{2.5}$ at a background site in central China, Atmos. Res., 239, 104881, https://doi.org/10.1016/j.atmosres.2020.104881, 2020.

Xu, K., Yin, L., Chen, Q., Liao, D., Ji, X., Zhang, K., Wu, Y., Xu, L., Li, M., Fan, X., Zhang, F., Huang, Z., Chen, J., and Hong, Y.: Quantitative analysis of influencing factors to aerosol pH and its responses to $PM_{2.5}$ and O_3 pollution in a coastal city, J. Environ. Sci., 151, 284–297, https://doi.org/10.1016/j.jes.2024.03.044, 2025.

Ye, X., Tao, Y., Liu, Y., Wang, R., Li, Q., Yang, X., and Chen, J.: Size-fractionated water-soluble ions during autumn and winter: Insights into volatile ammonium formation mechanisms in Shanghai, a megacity of China, Atmos. Environ., 2, 100011, https://doi.org/10.1016/j.aeaoa.2019.100011, 2019.

Zhang, B., Shen, H., Liu, P., Guo, H., Hu, Y., Chen, Y., Xie, S., Xi, Z., Skipper, T. N., and Russell, A. G.: Significant contrasts in aerosol acidity between China and the United States, Atmos. Chem. Phys., 21, 8341–8356, https://doi.org/10.5194/acp-21-8341-2021, 2021a.

Zhang, Q., Shen, Z., Lei, Y., Zhang, T., and Zhang, R.: Optical properties and source identification of black carbon and brown carbon: Comparison of winter and summer haze episodes in Xi'an, northwest China, Environ. Sci.: Processes Impacts, 21, 2058–2069, 2019.

Zhang, R., Han, Y., Shi, A., Sun, X., Yan, X., Huang, Y., and Wang, Y.: Characteristics of ambient ammonia and its effects on particulate ammonium in winter of urban Beijing, China, Environ. Sci. Pollut. Res., 28, 62828–62838, https://doi.org/10.1007/s11356-021-14108-w, 2021b.

Zhang, T., Shen, Z., Su, H., Liu, S., Zhou, J., Zhao, Z., Wang, Q., Prévôt, A. S. H., and Cao, J. J.: Effects of aerosol water content

on the formation of secondary inorganic aerosol during a winter heavy $PM_{2.5}$ pollution episode in Xi'an, China, Atmos. Environ., 252, 118304, https://doi.org/10.1016/j.atmosenv.2021.118304, 2021c.

Zhang, Y., Cai, J., Wang, S., He, K., and Zheng, M.: Review of receptor-based source apportionment research of fine particulate matter and its challenges in China, Sci. Total Environ., 586, 917–929, https://doi.org/10.1016/j.scitotenv.2017.02.071, 2017.

Zheng, G., Su, H., Wang, S., Andreae, M., Pöschl, U., and Cheng, Y.: Multiphase buffer theory explains contrasts in atmospheric aerosol acidity, Science, 369, 1374–1377, https://doi.org/10.1126/science.aba3719, 2020.

Zheng, G., Su, H., and Cheng, Y.: Role of carbon dioxide, ammonia, and organic acids in buffering atmospheric acidity: The distinct contribution in clouds and aerosols, Environ. Sci. Technol., 57, 12571–12582, https://doi.org/10.1021/acs.est.2c09851, 2023.

Zhou, M., Zheng, G., Wang, H., Qiao, L., Zhu, S., Huang, D., An, J., Lou, S., Tao, S., Wang, Q., Yan, R., Ma, Y., Chen, C., Cheng, Y., Su, H., and Huang, C.: Long-term trends and drivers of aerosol pH in eastern China, Atmos. Chem. Phys., 22, 13833–13844, https://doi.org/10.5194/acp-22-13833-2022, 2022.